

# Optimization for output power and band width in out-of-plane vibration energy harvesters employing electrets theoretically, numerically and experimentally

Chunhui Gao<sup>1</sup> · Shiqiao Gao<sup>1</sup> · Haipeng Liu<sup>1</sup> · Lei Jin<sup>1</sup> · Junhu Lu<sup>1</sup> · Ping Li<sup>2</sup>

Received: 9 February 2017 / Accepted: 4 April 2017 / Published online: 9 April 2017  
© Springer-Verlag Berlin Heidelberg 2017

**Abstract** In order to improve the performances of out-of-plane electret-based vibration energy harvesters (E-VEHs) in practical environment, we investigated the dependence of output power, resonance frequency and half power bandwidth on the load resistance for E-VEHs theoretically, numerically and experimentally. A linear analytical model is presented to describe the characteristics of E-VEHs qualitatively and the frequency response function of current versus acceleration excitation is obtained by Fourier transform when the ratio of mass amplitude to air gap is less than 0.28. In particular, the coupling effect of the electrostatic force not only changes E-VEHs' effective stiffness but also changes its effective damping. The analytical and numerical investigation predicted the following results: (1) an optimum value exists in the load resistance to maximize the output power; (2) enhanced electrostatic forces with decreasing the load resistance emphasize the soft spring effect, which lowers the resonance frequency; (3) a load resistance exists to maximize the half power bandwidth. A small out-of-plane E-VEHs prototype was fabricated in this paper in order to verify our predictions. The experimental results showed behaviors consistent with the numerical predictions. The output power reach a maximum 0.028 mW during frequency up-sweep and 0.0274 mW during frequency down-sweep at optimum load resistance 60 M $\Omega$  when the external acceleration were 1 ms<sup>-2</sup> and

82.3 Hz, respectively. When increasing the load resistance to 330 M $\Omega$ , the half power bandwidth increased to 3.1 Hz during frequency up-sweep and 3.2 Hz during frequency down-sweep, increased 58.8 and 52.9% over optimum load resistance 60 M $\Omega$ , respectively. The peak output power at load resistance 330 M $\Omega$  was 0.0187 mW during frequency up-sweep and 0.0179 mW during frequency down-sweep, when the external acceleration were 1 ms<sup>-2</sup> and 82.3 Hz, respectively. Therefore, the load resistance should be placed between 60 and 330 M $\Omega$ , while ensuring a higher output power can also get a larger bandwidth in practical applications.

## 1 Introduction

Since wireless sensor networks and low power devices have experienced remarkable growth in recent years, which raises the possibility of harvesting energy of the environment to replace the chemical batteries that raise maintenance, environment and size issues currently (Ling et al. 2013; Karami and Inman 2012; Roseveare and Natarajan 2013). Therefore, research has recently been focused on harvesting mechanical energy, especially on converting vibration energy into electric energy, and three mechanisms have been proposed: piezoelectric, electromagnetic and electrostatic (Harne and Wang 2013; Mitcheson et al. 2007; Li et al. 2014; Crovetto et al. 2014). Compared with piezoelectric and electromagnetic energy harvesters, the electrostatic systems have advantages of both compatibility with MEMS processes and small size. Using variable capacitors, induced charges from an external voltage bias (Paracha et al. 2009) or pre-charged (Sakane et al. 2008; Sterken et al. 2007; Wen Lo et al. 2008; Naruse et al. 2009; Crovetto et al. 2013; Wang and Hansen 2013) electrets can

✉ Chunhui Gao  
dzjdchunhui@126.com

<sup>1</sup> State Key Laboratory of Explosion Science and Technology, Beijing Institute of Technology, 100081 Beijing, People's Republic of China

<sup>2</sup> China Aerospace Science and Industry Corp, 100854 Beijing, People's Republic of China

move back and forth through an external load and power is generated when proof mass structure resonates according to the vibration source.

Among, electret-based vibration energy harvesters (E-VEHs) can be divided into two types, in-plane (Miki et al. 2010; Renaud et al. 2013; Crovetto et al. 2014) and out-of-plane (Boisseau et al. 2011; Chiu and Lee 2012; Asanuma et al. 2013; Chiu and Lee 2012; Asanuma et al. 2015), depending on the vibration direction. In-plane E-VEHs operate under vibration parallel to the electrets surface, whereas out-of-plane E-VEHs do so under vibration normal to the electrets surface. Compared with out-of-plane E-VEHs, in-plane E-VEHs can achieve high air capacitance vibration by lowering the air gap without pull-in, in which the in-plane E-VEHs can output more power. However, the patterning processing for electrets lead to higher production costs. Out-of-plane E-VEHs have lower production costs because they lack this patterning process and are of a simple device structure. Driven by the merit of low production costs, more and more researchers focus on out-of-plane E-VEHs and attempt to improve their performances.

Because of the coupling equations of out-of-plane E-VEHs cannot be solved analytically, therefore some previous works had focused on improving the performances of out-of-plane E-VEHs by numerical optimization techniques. Boisseau et al. (2011) employed a silicon-based oscillator with a cantilever structure and Teflon FEP-based electrets numerically optimized the resistive load, the electrets length parallel to the beam, and the initial air gap between the oscillator and the electrets face. Chiu and Lee (2012) employed a flexible printed circuit and  $\text{Si}_3\text{N}_4/\text{Si}_3\text{N}_4/\text{SiO}_2\text{-SiO}_2$  bilayer electrets, numerically optimized the load resistance and the initial air gap. However, these previous efforts focused solely on enhancing the output power and did not closely investigate changes in the frequency bandwidths within the numerical optimization. Asanuma and Hara (2015) employed CYTOP electrets to optimize the initial air gap to maximize the output power and to widen the frequency bandwidth. But they neglected another important parameter that the load resistance not only changes the output power but also can adjust resonance frequency and frequency bandwidth of out-of-plane E-VEHs.

In this study, we investigate the dependence of output power, resonance frequency, and half power bandwidth on load resistance in out-of-plane E-VEHs, with the external acceleration and electrets surface potential held constant. First, the mechanical–electrical coupling model of out-of-plane E-VEHs is built. Second, the frequency response function of output power versus acceleration excitation is obtained by Fourier transform. At last, we numerically investigate the performances of the harvester, and then experimentally evaluate these optimal designs and

compare the real device performances with the numerically predictions.

## 2 Out-of-plane E-VEHs with double-clamped beam

An electrostatic harvester unit able to turn vibrations into electricity using electrets can be found in Fig. 1, it is composed of a counter-electrode and an electrode on which is deposited electrets, spaced by air gap and connected by electrical load (here a load resistance). The electrets have constant surface charges  $Q$ , due to electrical induction and charges conservation, the sum of charge on the electrode  $Q_b$  and on the counter-electrode  $Q_t$  equals the charges  $Q$  on electrets:

$$Q = Q_b + Q_t \quad (1)$$

When a vibration occurs, it induces a reorganization of charges between the electrode and the counter-electrode through the load resistance. This induces a current  $i$  across the load resistance and part of the mechanical energy is then turned into electricity.

The equivalent electrostatic model of the electrostatic converter is presented in Fig. 2. Where,  $V_s$  is the surface

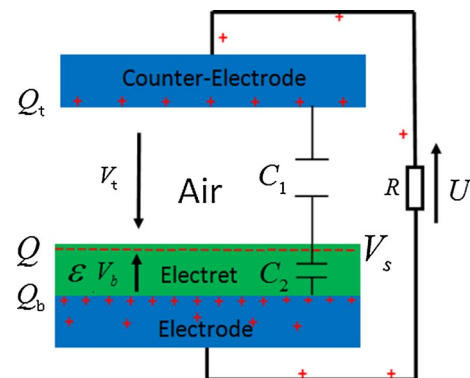


Fig. 1 Electrostatic converter using electrets

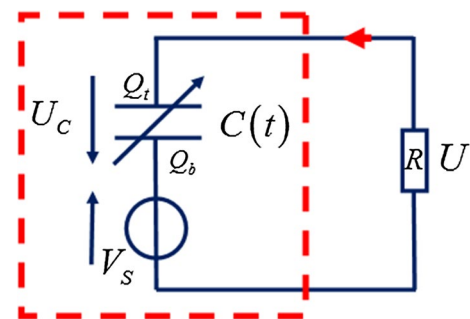


Fig. 2 Equivalent electric model of the electrostatic converter

voltage of electrets and  $C(t)$  is the capacitance between the counter-electrode and the electrode.  $C(t)$  corresponds to the serial capacitance formed by the constant capacitance  $C_2(C_2 = \epsilon_0 \epsilon_e A/d)$  of the electrets dielectric material and the variable capacitance  $C_1(t)(C_1(t) = \epsilon_0 A/(g_0 - x(t)))$  of the air gap. Kirchhoff's law gives the differential equation that governs the electrostatic system:

$$\frac{Q_b(t)}{C_2} - \frac{Q_t(t)}{C_1(t)} = U = R \frac{dQ_t(t)}{dt} \tag{2}$$

According to Eq. (1), Eq. (2) can be simplified to the following form:

$$\frac{V_s}{R} - \frac{Q_t(t)}{RC(t)} = \frac{dQ_t(t)}{dt} \tag{3}$$

Where,  $C(t) = \frac{\epsilon_0 A}{g_0 - x(t) + d/\epsilon_e}$ ,  $\epsilon_e$  is the relative permittivity of the electrets and  $\epsilon_0$  is the absolute permeability of air. And  $A$  represents the surface area of the electrets,  $g_0$  represents the initial air gap between the electret surface and the counter-electrode,  $d$  represents the thickness of the electrets and  $x(t)$  represents the transient displacement of the mass. Surface potential  $V_s (V_s = Q/C_2)$  could be considered as a monotonous linear function of charges  $Q$ .

E-VEHs is a typical type of vibration energy harvester can be modeled as a mobile mass suspended to a support by a spring and damped by forces. When a vibration occurs, it induces a relative displacement of the mobile mass compared to the frame showed in Fig. 3a.

In this paper, a small E-VEHs prototype was fabricated in order to verify our predictions. We employed a 300  $\mu\text{m}$  thick stainless steel film to fabricate a clamped-clamped beam oscillator. A 1.5 cm  $\times$  1.5 cm  $\times$  1 cm ceramic mass was added at the middle of the beam to increase the output power. A *PP* polymer electrets film (China. Shanghai

Electret Materials Technology Co. LTD) with  $-500$  V surface potential was prepared using the point-to-grid corona-discharge method. The charges are implanted onto a 30  $\mu\text{m}$  thick *PP* polymer film which was spin-coated on a rigid copper plate with the help of a copper double-tape. The copper foil was uniformly adhered to the surface of the ceramic body as a counter-electrode. As shown in Fig. 3b, the harvester was assembled and set on the shaker. A high speed photographer was used to measure the peak-to-peak amplitude of the centre of the oscillator.

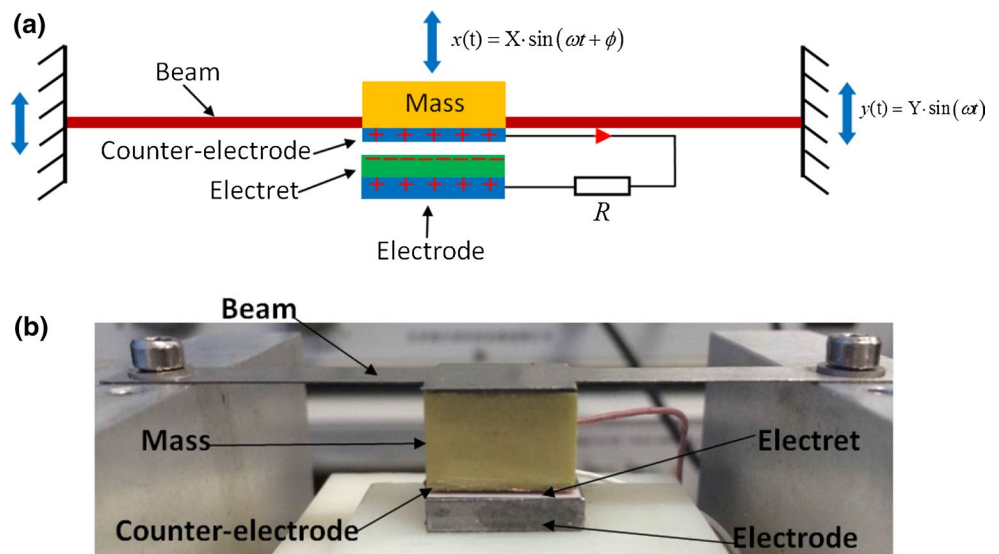
### 3 Analytical model of out-of-plane E-VEHs

To analyze the main performances of out-of-plane E-VEHs and to identify the load resistance's effect, it is necessary to find coupled mechanical and electrostatic equations that rule the out-of-plane E-VEHs. The double-clamped beam with a mass at its middle can be modeled as a damped mass-spring structure. The mechanical friction force means the material energy dissipation of the beam can be modeled as viscous force and the electrostatic force is the derivative of the electrostatic energy of the capacitor  $W_e$  with respect to the displacement  $x(t)$ .  $W_e$  is equal to the charge on the upper electrode  $Q_t$  squared, divided by twice the capacitance as a function of time  $C(t)$ . Therefore, the mechanical system is ruled by:

$$m\ddot{x}(t) + b\dot{x}(t) + kx(t) - \frac{d}{dx} \left( \frac{1}{2} \frac{Q_t^2}{C(t)} \right) - mg = ma(t) \tag{3}$$

$$\frac{dQ_t(t)}{dt} = \frac{V_s}{R} - \frac{Q_t(t)}{RC(t)} \tag{4}$$

**Fig. 3** Clamped-clamped E-VEHs. **a** Schematic diagram, **b** prototype



Where,  $V_s$  is the surface voltage of the electrets and  $C(t)$  is the capacitance between the counter-electrode and the electrode. Capacitance  $C(t)$  corresponds to the serial capacitance formed by the constant capacitance  $C_2$  of the electrets dielectric material and the variable capacitance  $C_1(t)$  of the air gap. Nevertheless, it is not possible to get an analytical expression for  $x(t)$  and  $Q_t(t)$ . Coincidentally, the V-EVHs output voltage is positively related to the amplitude of the mass, a linear model can be derived to describe the characteristics of the performances qualitatively when the amplitude of the mass is small. The charge  $Q_t(t)$  on movable electrode can be written as  $Q_t(t) = Q_{10} + \Delta Q_t(t)$ , where  $Q_{10} = Q / (1 + \frac{\epsilon_e g_0}{d})$  is the bias charge only related to the size of the structure. The charge  $Q_b(t)$  on fixed electrode can be written as  $Q_b(t) = Q_{20} - \Delta Q_t(t)$ , where  $Q_{20} = \frac{Q}{1 + \frac{\epsilon_e g_0}{d}}$  is the bias charge also only related to the size of the structure  $\Delta Q_t(t)$  is the time-varying component of  $Q_t(t)$  and  $Q_b(t)$  caused by the vibration, according to Eq. (2), a governing equation of  $\Delta Q_t(t)$  can be derived as follow:

$$\frac{Q_{20} + \Delta Q(t)}{C_2} - \frac{Q_{10} - \Delta Q(t)}{C_1(t)} = R \frac{d\Delta Q(t)}{dt} \tag{5}$$

Equation (5) is developed as follow:

$$\frac{x(t)}{g_0} + \frac{\Delta Q(t)}{Q_{10}} \frac{x(t)}{g_0} = \frac{\Delta \dot{Q}(t)}{Q_{10}} \frac{\epsilon_0 A R}{g_0} + \frac{\Delta Q(t)}{Q_{10}} \frac{d}{g_0 \epsilon_e} + \frac{\Delta Q(t)}{Q_{10}} \tag{6}$$

Since both  $\Delta Q(t)$  and  $x(t)$  are the amount of change over time and smaller than  $Q_{10}$  and  $g_0$ ,  $\Delta Q(t)$  is a function of  $x(t)$ . When  $x(t)$  is small relative to  $g_0$ , the second term on the left side of the above Eq. (6) can be ignored, a linear equation can be obtained:

$$R \frac{d\Delta Q_t(t)}{dt} + \frac{\Delta Q_t(t)}{C_0} = E_{10} x(t) \tag{7}$$

where,  $C_0 = \epsilon_0 A (g_0 + d/d\epsilon_e)$  and  $E_{10} = Q_{10}/\epsilon_0 A$  are the dc components of the capacitance  $C(t)$  and the electric field in the gap, respectively.

Therefore, the mechanical system can be modified as follow:

$$m \ddot{x}(t) + b \dot{x}(t) + kx(t) - E_{10} \Delta Q_t(t) = ma(t) + \frac{1}{2} Q_{10} E_{10} + mg \tag{8}$$

By means of Fourier transform, time-varying component of charge induced on the counter-electrode is derived from the Eq. (8):

$$\Delta \tilde{Q}_1(\omega) = \frac{E_{10} C_0}{1 + j\omega RC_0} \tilde{x}(\omega) \tag{9}$$

Where,  $\omega$  is the excitation frequency. Similarly, frequency response function of amplitude versus acceleration excitation can be obtained by Fourier transform, which is expressed as:

$$\frac{\tilde{x}(\omega)}{\tilde{a}(\omega)} = \frac{m}{-m\omega^2 + k - \frac{E_{10}^2 C_0}{(1 + (\omega RC_0)^2)} + j\omega \left( b + \frac{E_{10}^2 C_0^2 R}{(1 + (\omega RC_0)^2)} \right)} \tag{10}$$

Then the amplitude of mass at any frequency  $\omega$  is:

$$x_M = \frac{m a_M}{\sqrt{\left[ -m\omega^2 + k - \frac{E_{10}^2 C_0}{(1 + (\omega RC_0)^2)} \right]^2 + \left[ \omega \left( b + \frac{E_{10}^2 C_0^2 R}{(1 + (\omega RC_0)^2)} \right) \right]^2}} \tag{11}$$

$a_M$  is the amplitude of external acceleration. As illustrated in Eq. (11), the vibration characteristics of the out-of-plane E-VEHs are affected by the electrostatic force. In particular, the coupling effect of the electrostatic force not only changes the effective stiffness but also changes the effective damping. Thus, the effective stiffness and effective damping coefficient of the energy harvester at any excitation frequency  $\omega$  are shown, respectively, as

$$k_{eff} = k - \frac{E_{10}^2 C_0}{(1 + (\omega RC_0)^2)} \tag{12}$$

$$b_{eff} = b + \frac{E_{10}^2 C_0^2 R}{(1 + (\omega RC_0)^2)} \tag{13}$$

The current  $|I|$  flows through resistance load  $R$  is

$$|I| = \frac{\omega E_{10} C_0}{\sqrt{1 + (\omega RC_0)^2}} x_M \tag{14}$$

Thus, the output power of the out-of-plane E-VEHs can be calculated by

$$P_{out} = \frac{R \omega^2 E_{10}^2 C_0^2}{2 + 2(\omega RC_0)^2} x_M^2 \tag{15}$$

Now, we solve Eqs. (11), (12), (13), and (15) by substituting parameters found in Table 1, and evaluate the mass amplitude, effective damping, effective stiffness,

**Table 1** Fixed parameters of out-of-plane E-VEHs

Parameters	Designation	Value
$k$	Stiffness	5400 N/m
$c$	Damping	0.325 N/(m/s)
$M_{electret}$	Material of the electrets	PP
$m$	Mobile mass	20 g
$V_s$	Surface potential	-500 V
$S$	Electrets surface area	15 mm × 15 mm
$a$	External acceleration amplitude	1 m s <sup>-2</sup>
$\epsilon_r$	Dielectric constant of the electrets	2.2
$d$	Electrets thickness	30 μm
$g_0$	Initial air gap	300 μm

and frequency bandwidth of the E-VEHs. For simplicity of the calculation, this study employed the constant viscous damping obtained from the experimental value of the damping coefficient and natural frequency. We measured these values using the same mechanical vibrating system as shown in Fig. 3 but without the charging PTFE polymer by using free decay oscillation method with the help of high speed photography.

Figure 4 shows theoretical analysis of performances of E-VEHs with versus load resistance when the initial air gap  $g_0 = 300 \mu\text{m}$  and the external acceleration were  $1 \text{ ms}^{-2}$ . The effective damping increased from 0.325 N/(m/s) without electret with respect to the load resistance increased until reaching a maximum 0.343 N/(m/s) at 290 M $\Omega$  then decreased as Fig. 4a. The effective stiffness decreased with respect to the load resistance increased in the whole process as Fig. 4b shows. Similar with effective damping, an optimal load existed to reach the maximum output power at 270 M $\Omega$ . Despite the analytical results maybe not

very accurate compared with simulation results, but it can describe the characteristics of E-VEHs qualitatively.

### 4 Numerical results of performances

Next, we will numerically solve the differential Eqs. (3) use Matlab/Simulink by substituting parameters found in Table 1 to evaluate the output power, resonance frequency, and frequency bandwidth of the E-VEHs.

In addition to initial air gap, load resonance is another important parameter for out-of-plane E-VEHs which have been overlooked by previous works. Output power  $P_{out}$  and the mass absolute amplitude  $x_M$  with respect to load resistance were given in Fig. 4c, d. There exists an optimal load resistance to reach maximum power, different from output power  $P_{out}$ , there also exists a load resistance to impede the amplitude  $x_M$  to reach the minimum value to obtain a maximum bandwidth. Load resistance changes

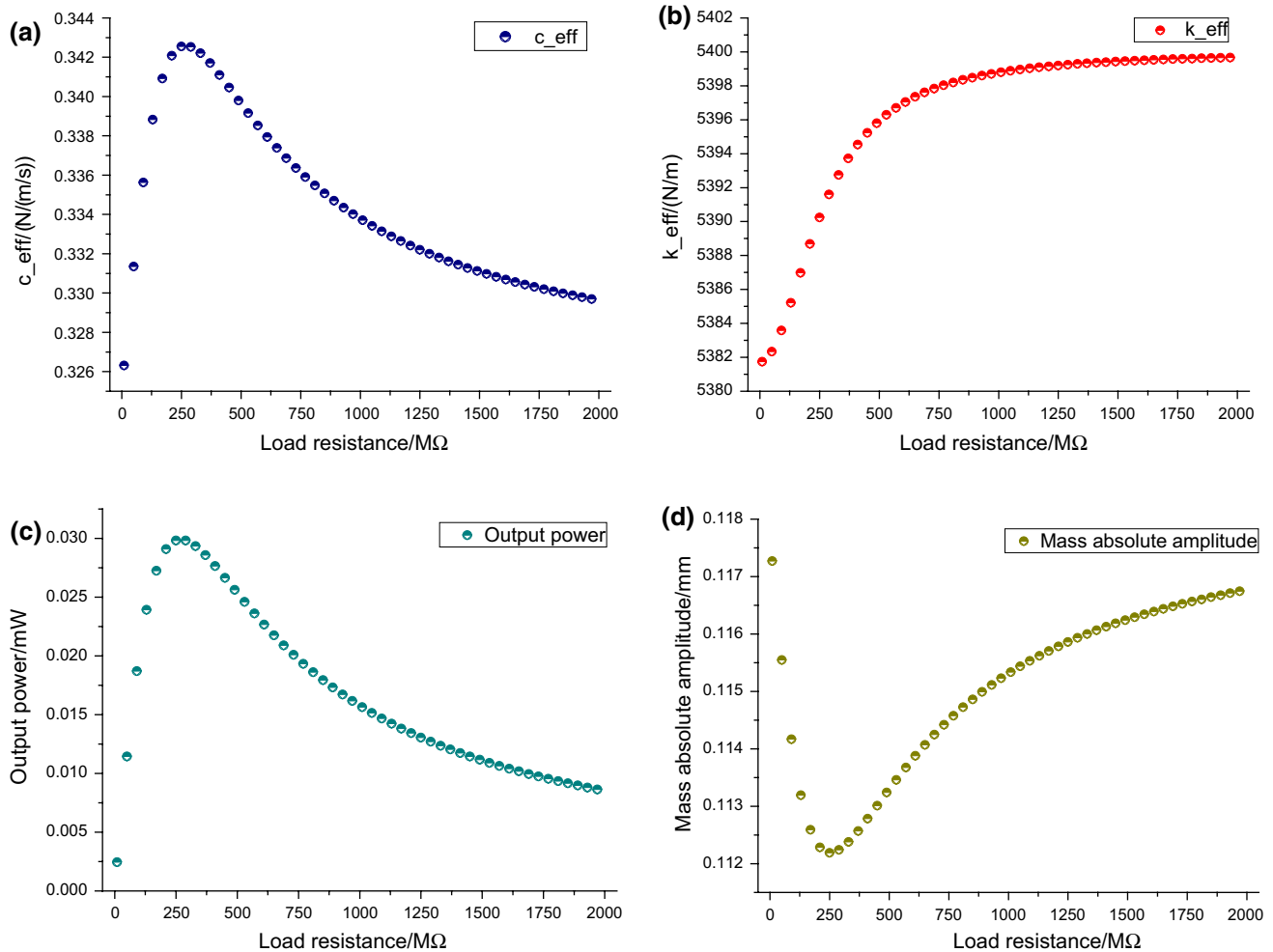


**Fig. 4** Performances of E-VEHs with respect to load resistance **a** effective damping, **b** effective stiffness, **c** output power, **d** mass absolute amplitude

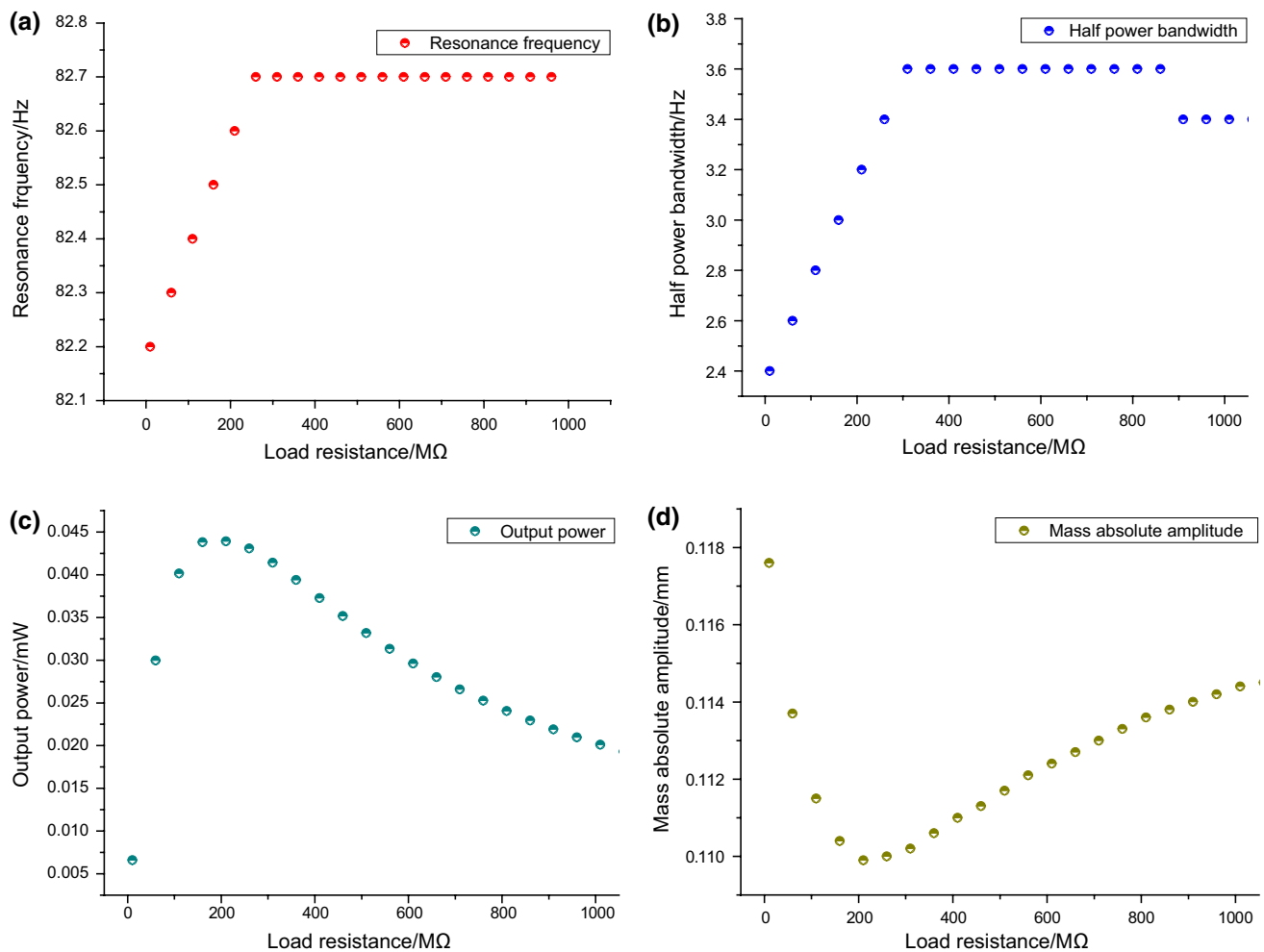
harvester's performances by charging the electrostatic force  $F_{elec}$  between the electrets and the counter-electrode. Electrostatic force  $F_{elec}$  is a complex periodic function under periodic external excitation so that it's hard to describe in previous studies. But according to Eq. (8),  $F_{elec}$  can be divided into two parts, constant electrostatic force  $F_{static}$  and variable electrostatic force  $F(t)$ . Constant electrostatic force  $F_{static}$  works with gravity of mass together change the initial air gap which had been described detailed in H Asanuma's (Chiu and Lee 2012) work. Variable electrostatic force  $F(t)$  can be divided into two parts also, viscous electrostatic force  $F_c(t)$ , which changes E-VEHs' damping coefficient, and elastic electrostatic force  $F_k(t)$ , which changes E-VEHs' stiffness. Therefore, viscous electrostatic force  $F_c(t)$  affects E-VEHs' half power bandwidth and electrostatic force  $F_k(t)$  affects E-VEHs' resonance frequency.

Figure 5 shows the simulation performances of E-VEHs with versus load resistance when the initial air gap  $g_0 = 300 \mu\text{m}$  and the external acceleration were  $1 \text{ ms}^{-2}$ .

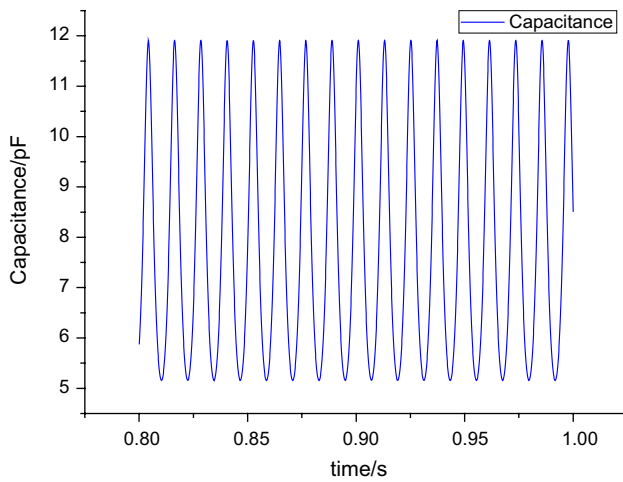
The resonance frequency decreased with load resistance decreased, but the half power bandwidth's variation trend looks more attractive than the resonance frequency drift. There exists a load resistance to reach the maximum half power bandwidth, the half power bandwidth reaches a maximum and then decreased with further increases load resistance. The half power bandwidth  $\Delta f$  reaches a maximum 3.6 Hz at  $R = 310 \text{ M}\Omega$ , and  $\Delta f = 3.2 \text{ Hz}$  when the output power reach maximum at  $R = 218 \text{ M}\Omega$ .

Figure 5c gives output power with respect to load resistances at resonance frequency. When electret size, initial air gap, and external acceleration held constant, the output power reached a maximum of 0.044 mW at 218 M $\Omega$  and 0.0414 mW at 310 M $\Omega$  when bandwidths reach maximum. When load resistance was changed from 218 to 310 M $\Omega$ , the output power is reduced 5.9%, but half power bandwidth is increased 18.75%.

There exists difference of maximum output load resistance between analytical and simulation results as we can



**Fig. 5** Numerical results of the **a** resonance frequency and, **b** half power bandwidth with respect to load resistance, **c** output power at resonance frequency as load resistance increases, **d** mass absolute amplitude at resonance frequency as load resistance increases



**Fig. 6**  $C(t)$  change along with time

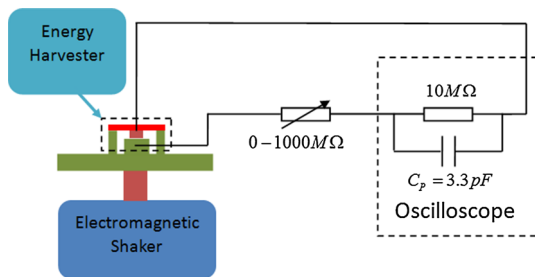


**Fig. 7** Equipment of measuring output voltage

see in Figs. 4c and 5c. To maximize the power output delivered to the load resistance in the analytical model, the two impedances,  $R$  and  $1/(\omega C_0)$ , should be matched. When  $g_0 = 0.3$  mm,  $C_0 = 7.2$  pF. When the excitation frequency  $f$  is 82.7 Hz,  $1/(\omega C_0) \approx 270$  MΩ. In the simulation model,  $C(t)$  is a quantity that changes over time as Fig. 6 shows:

The capacitance curve is not a standard positive or cosine curve. The average capacitance  $C(t)_m$  is 8.8 pF, When the excitation frequency  $f = 82.7$  Hz,  $1/(\omega C(t)_m) \approx 218$  MΩ.

### 5 Experiment results and discussions

Here, we will experimentally investigate the numerical predictions that (1) an optimal value for load resistance to maximize the output power, (2) the half power bandwidth exists an maximum as load resistance increases, (3) resonance frequency decreases as load resistance increases. The parameters used in experiment are the same values as used in the numerical investigation, showed in Table 1.

In order to test output characteristics of eletret-based energy harvester and validate the analytical calculation results, a out-of-plane E-VEHs prototype was fabricated.

First, some inherent characteristics of the damped mass-spring structure are measured by free decay oscillation method with the help of high speed photography. The damped mass-spring structure’s natural frequency is 82.6 Hz. The equivalent measuring output voltage circuit refers to Fig. 7, experimental setup shows in Fig. 8a. The output voltage is measured on the 10 MΩ internal impedance (with 3.3 pF parasitic capacitance) of the probe in series with the load resistance. The whole setup of the device is mounted on the vibrating shaker which is connected to a signal generator through a power amplifier. Lead wire from the electrode is connected across a load resistance to counter-electrode. The current generated in the circuit due to external vibration is captured by an oscilloscope. In addition, an accelerometer is used to record vibration acceleration. A load resistance box contained five 1 MΩ load resistances, five 10 MΩ load resistances, five 100 MΩ load resistances, a 5 MΩ load resistance, a 50 MΩ load resistance, and a 500 MΩ load resistance was assembled as Fig. 8b. The load resistance box allowed us obtain a variable load resistance range from 1 to 1000 MΩ.

Figure 9a shows the experimental output voltage amplitude of  $R = 10$  MΩ during frequency sweep up and down when the initial air gap  $g_0 = 300$  μm under  $1$  m/s<sup>2</sup> external acceleration. It shows that the nonlinear of double-beam in our experiment is not obvious for small displacement. So we ignore the nonlinear stiffness of double-beam in the aforementioned dynamical equation is reasonable. Figure 9b shows the output voltage amplitude of  $R = 10$  MΩ varies with acceleration amplitude when the initial air gap  $g_0 = 300$  μm. When the acceleration amplitude is less than  $0.7$  m/s<sup>2</sup>, the voltage value obtained by the Eq. (7) is consistent with the simulation result and the experimental result, and the voltage amplitude is linearly related to the acceleration amplitude. When the acceleration amplitude is greater than  $0.7$  m/s<sup>2</sup>, the voltage amplitude obtained by Eq. (7) is smaller than that obtained by simulation and experiment, because the nonlinearity of the system becomes more and more obvious as the acceleration amplitude increases and the Eq. (7) is no longer applicable as a linear equation. Therefore, when the ratio of the amplitude of the mass to the air gap is less than 0.28, the theoretical model given in this paper is established.

Figure 10 shows experimental output power, half power bandwidth, resonance frequency, and mass amplitude of out-of-plane E-VEHs when the external acceleration is  $1$  ms<sup>-2</sup> corresponding to the numerical predictions shown in Fig. 5. An optimal load resistance  $R = 60$  MΩ exists to reach the maximum output power 0.028 mW during frequency up-sweep and 0.0274 mW during frequency down-sweep. The half power bandwidth reach a maximum  $\Delta f = 3.1$  Hz during frequency up-sweep and a maximum  $\Delta f = 3.2$  Hz during frequency down-sweep

**Fig. 8** **a** Experimental setup, **b** load resistance box

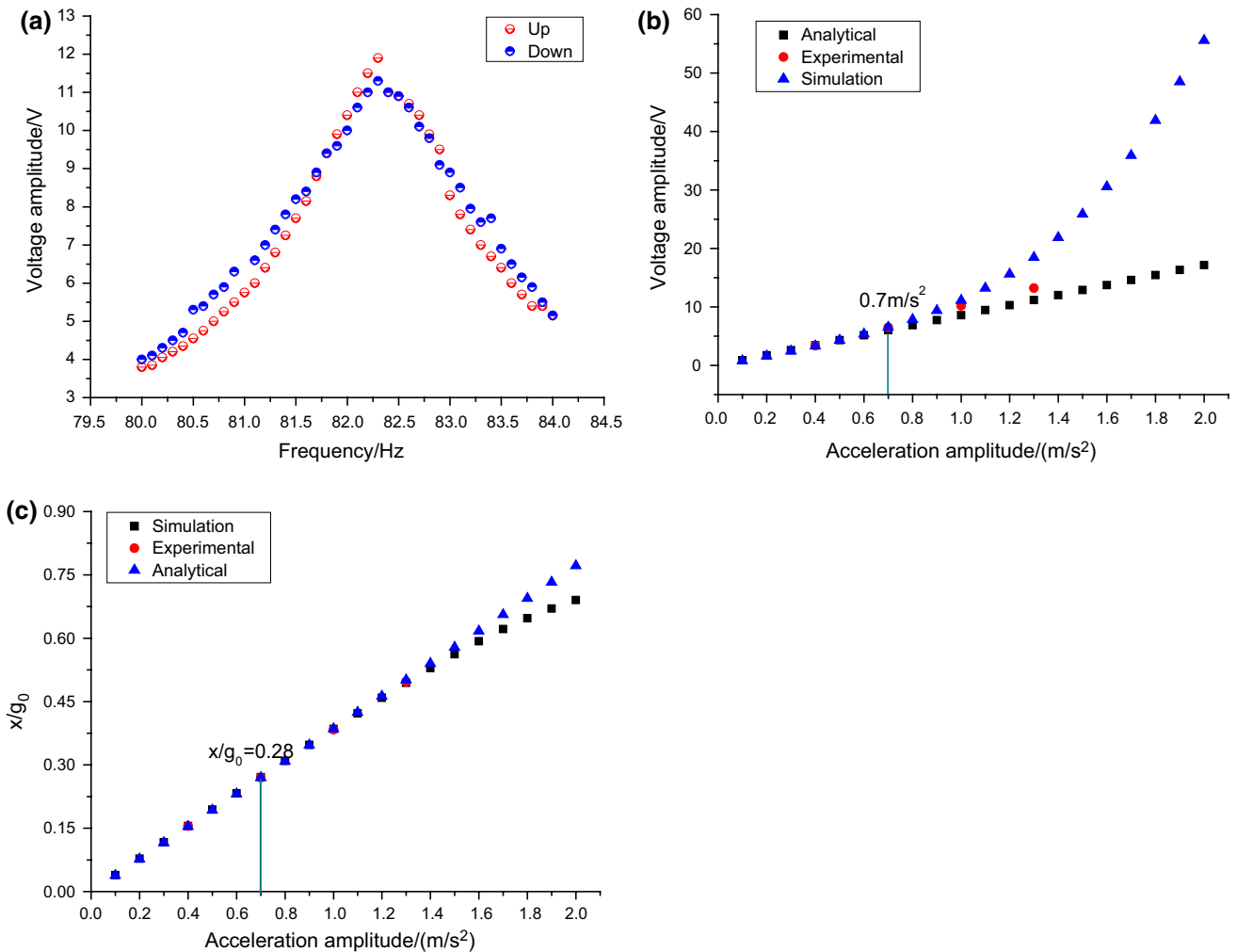
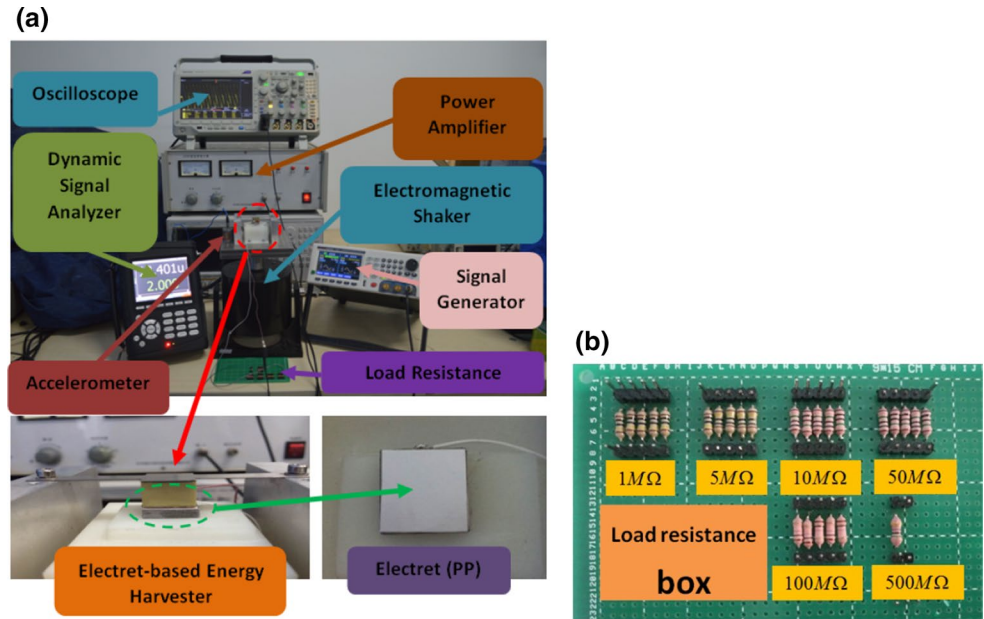


**Fig. 9** **a** Output voltage amplitude varies with frequency experimental, **b** output voltage amplitude varies with acceleration amplitude analytical, numerical and experimental, **c** normalized mass amplitude varies with acceleration amplitude analytical, numerical and experimental



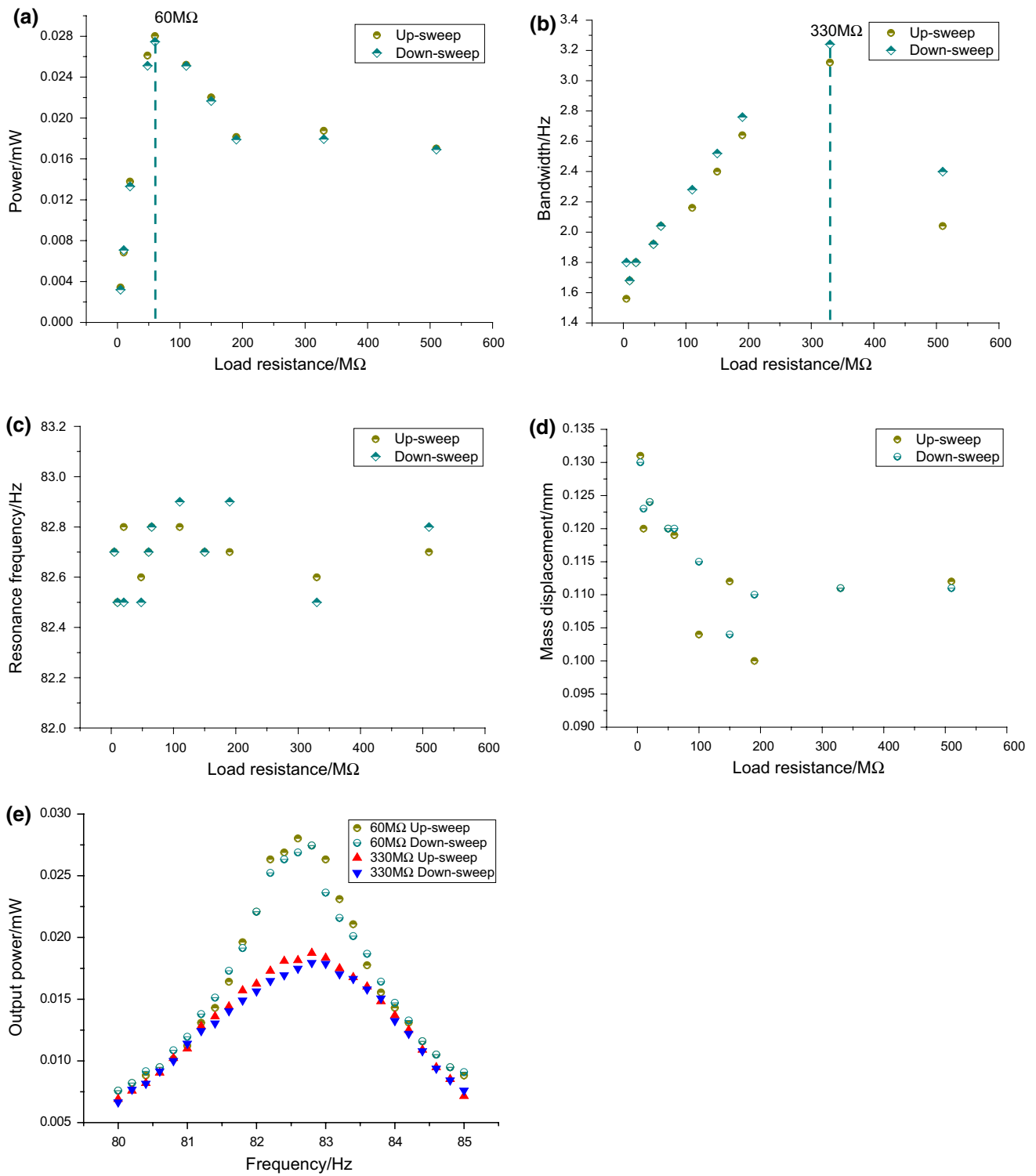


**Fig. 10** Experimental results of **a** output power, **b** half power bandwidth, **c** resonance frequency, **d** mass amplitude respect to load resistance, **e** power respect to frequency sweep

when load resistance  $R = 330 \text{ M}\Omega$ . But, the variations of resonance frequency are not obvious when load resistance increases from 10 to 510 MΩ, the maximum frequency

drift is less than 0.5%. When the load resistance increases from 60 to 330 MΩ, the half power bandwidth increases 58.8% during frequency up-sweep and 52.9% during

frequency down-sweep, output power decreases 33.2% during frequency up-sweep and 34.6% during frequency down-sweep, respectively. However, the narrow half power bandwidth is not good for practical use, since E-VEHs desperately require wider half power bandwidth, as well as higher output power. Therefore, the load resistance should be placed between 60 and 330 M $\Omega$ , while ensuring a higher output power can also get a larger bandwidth in practical applications.

While similar overall trends were seen, there exist large discrepancies between the absolute values of output power for the numerical and experimental results. The difference of output power results from surface potential decay of PP electrets and a parasitic capacitance built into the experiment step especially when using high-value resistors. Because E-VEHs' output power is positively related to the square of the surface potential. A slight potential decay of PP electrets' surface potential will greatly reduce the output power. The maximum capacitance variation of our E-VEHs type remains only 11.9 pF. Thus, a parasitic capacitance, even with only several decades pF, will significantly decrease the relative capacitance variation and thus the output power. Despite the large differences between the absolute values of output power for the numerical and experimental results, but it but does not obstruct our main conclusions in this paper: (1) an optimum value exists in the load resistance to maximize the output power; (2) enhanced electrostatic forces with decreasing the load resistance emphasize the soft spring effect, which lowers the resonance frequency; (3) a load resistance exists to maximize the half power bandwidth; (4) the load resistance should be placed between maximum power load resistance and maximum bandwidth load resistance, while ensuring a higher output power can also get a larger bandwidth in practical applications.

## 6 Conclusions

In this paper, we have presented an investigation of load resistance optimization for output power and half power bandwidth in out-of-plane electret-based vibration energy harvesters. First, an analytical model of small signal is presented to describe the characteristics of out-of-plane E-VEHs. Then, the frequency response function of current versus acceleration excitation was obtained by Fourier transform. In particular, the coupling effect of the electrostatic force not only changes the system's effective stiffness but also changes its effective damping. Second, We investigated the dependence of output power, resonance frequency and half power bandwidth on the load resistance for electret-based out-of-plane vibration energy harvesters, both numerically and experimentally. The numerical

investigation predicted the following results: (1) an optimum value exists in the load resistance to maximize the output power; (2) enhanced electrostatic forces with decreasing the load resistance emphasize the soft spring effect, which lowers the resonance frequency; (3) a load resistance exists to maximize the half power bandwidth. The experimental results showed behaviors consistent with the numerical predictions. The output power reach a maximum 0.028 mW during frequency up-sweep and 0.0274 mW during frequency down-sweep at optimum load resistance 60 M $\Omega$  when the external acceleration were 1 ms<sup>-2</sup> and 82.3 Hz, respectively. When increasing the load resistance to 330 M $\Omega$ , the half power bandwidth increased to 3.1 Hz during frequency up-sweep and 3.2 Hz during frequency down-sweep, increased 58.8 and 52.9% over optimum load resistance, respectively. The peak output power at load resistance 330 M $\Omega$  was 0.0187 mW during frequency up-sweep and 0.0179 mW during frequency down-sweep, when the external acceleration were 1 ms<sup>-2</sup> and 82.3 Hz, respectively. Therefore, the load resistance should be placed between maximum power load resistance and maximum bandwidth load resistance, while ensuring a higher output power can also get a larger bandwidth in practical applications.

**Acknowledgements** This project is supported by the National High Technology Research and Development Program of China (Grant No. 2013AA041104).

## References

- Asanuma H, Oguchi H, Hara M et al (2013) Ferroelectric dipole electrets for output power enhancement in electrostatic vibration energy harvesters[J]. *Appl Phys Lett* 103(16):162901
- Asanuma H, Hara M, Oguchi H et al (2015) Air gap optimization for output power and band width in out-of-plane vibration energy harvesters employing electret[J]. *J Micromech Microeng* 25(10):104013
- Boisseau S, Despesse G, Ricart T, Defay E, Sylvestre A (2011) Cantilever-based electret energy harvesters. *Smart Mater Struct* 20(1):105013
- Chiu Y, Lee YC (2012) Flat and robust out-of-plane vibrational electret energy harvester[J]. *J Micromech Microeng* 23(1):015012
- Crovetto A, Wang F, Hansen O (2013) An electret-based energy harvesting device with a wafer-level fabrication process. *J Micro-mech Microeng* 23(11):114010
- Crovetto A, Wang F, Hansen O (2014) Modeling and optimization of an electrostatic energy harvesting device. *J Microelectromech Syst* 23(5):1141–1155
- Harne RL, Wang KW (2013) A review of the recent research on vibration energy harvesting via bistable systems. *Smart Mater Struct* 22:023001
- Karami MA, Inman DJ (2012) Powering pacemakers from heartbeat vibrations using linear and nonlinear energy harvesters. *Appl Phys Lett* 100:042901
- Li P, Gao S, Niu S et al (2014) An analysis of the coupling effect for a hybrid piezoelectric and electromagnetic energy harvester. *J Smart Mater Struct* 23(6):065016

- Ling CS, Dan H, Steve GB (2013) Technological challenges of developing wireless health and usage monitoring systems. *Proc SPIE* 8695:86950K
- Lu Y, O’Riordan E, Cottone F et al (2016) A batch-fabricated electret-biased wideband MEMS vibration energy harvester with frequency-up conversion behavior powering a UHF wireless sensor node[J]. *J Micromech Microeng* 26(12):124004
- Miki D, Honzumi M, Suzuki Y et al (2010) IEEE 23rd Int. Conf. on Micro Electro Mechanical Systems (Wanchai), pp 176–179
- Mitcheson PD, Green TC, Yeatman EM (2007) Power processing circuits for electromagnetic, electrostatic and piezoelectric inertial energy scavengers. *Microsyst Technol* 13:1629–1635
- Naruse Y, Matsubara N, Mabuchi K, Izumi M, Suzuki S (2009) Electrostatic micro power generation from low-frequency vibration such as human motion. *J Micromech Microeng* 19(9):094002
- Paracha A, Basset P, Galayko D, Marty F, Bourouina T (2009) A silicon MEMS DC/DC converter for autonomous vibration-to-electrical-energy scavenger. *IEEE Electron Device Lett* 30(5):481–483
- Renaud M, Altena G, Goedbloed M et al (2013) Proc. 17th Int. Conf. on Solid-State Sensors, Actuators and Microsystems (Barcelona), pp 693–696
- Roseveare N, Natarajan B (2013) A structured approach to optimization of energy harvesting wireless sensor networks Proc. IEEE Conf. on Consumer Communications and Networking (Las Vegas NV, Jan. 2013) pp 420–5
- Sakane Y, Suzuki Y, Kasagi N (2008) The development of a high-performance perfluorinated polymer electret and its application to micro power generation. *J Micromech Microeng* 18(10):104011
- Sterken T, Fiorini P, Altena G, Van Hoof C, Puers R (2007) Harvesting energy from vibrations by a micromachined electret generator. In Proc. Int. Conf. Solid-State Sens., Actuators, Microsyst, pp. 129–132
- Wang F, Hansen O (2013) Invisible surface charge pattern on inorganic electrets. *IEEE Electron Device Lett* 34(8):1047–1049
- Wen Lo H, Tai Y-C (2008) Parylene-based electret power generators. *J Micromech Microeng* 18(10):104006
- Zhang Y, Luo A, Xu Y et al (2016) Electret-based electrostatic energy harvesting device with the MEMS technology[C]//Mechatronic and Embedded Systems and Applications (MESA), 2016 12th IEEE/ASME International Conference on. IEEE, 1–6